Journal of the Korean Physical Society, Vol. 45, No. 2, August 2004, pp. 287∼294

Noise Effect on Weak Chaotic Synchronization in Coupled Invertible Systems

Woochang Lim* and Sang-Yoon Kim
Department of Physics, Kangwon National University, Chunchon 200-701

(Received 16 March 2004)

We investigate the noise effect on weak chaotic synchronization in coupled invertible systems such as coupled Hénon maps and coupled pendula. Weakly stable synchronous chaotic attractors (SCAs) with positive local transverse Lyapunov exponents are sensitive with respect to variations in the noise intensity. To quantitatively characterize such noise sensitivity, we generalized the method proposed in coupled one-dimensional noninvertible maps to coupled high-dimensional invertible systems. Thus, we introduce a quantifier, called the noise sensitivity exponent (NSE), to measure the "degree" of the noise sensitivity and to characterize the effect of noise on the bubbling and the riddling of a weakly stable SCA. Such a noise effect is found to be the same as the effect of parameter mismatch between subsystems.

PACS numbers: 05.45.Xt
Keywords: Chaos synchronization, Noise effect

I. INTRODUCTION

In recent years, due to its potential practical applications, synchronization in coupled chaotic systems has become a field of intensive study [1]. For the case of chaos synchronization, a synchronous chaotic attractor (SCA) exists on an invariant subspace of the whole phase space [2]. If the SCA is stable against a perturbation transverse to the invariant subspace, it may become an attractor in the whole phase space. Properties of transverse stability of the SCA are intimately associated with transverse bifurcations of periodic saddles embedded in the SCA [3–8]. If all periodic saddles are transversely stable, the SCA becomes asymptotically stable. For this case, we have "strong" synchronization. However, as the coupling parameter passes through a threshold value, a periodic saddle first becomes transversely unstable through a local bifurcation. After this first transverse bifurcation, trajectories may be locally repelled from the invariant subspace when they visit the neighborhood of a transversely unstable periodic repeller. Thus, loss of strong synchronization begins with the first transverse bifurcation, and then we have "weak" synchronization. For this case, intermittent bursting [9,10] or basin riddling [11] occurs, depending on the global dynamics. For the bursting case, locally repelled trajectories from the invariant synchronization subspace are restricted to move within a bounded region and exhibit transient intermittent bursting. On the other hand, for the riddling case, the locally repelled trajectories will go to another attractor (or infinity); hence, the basin of attraction becomes riddled with a dense set of "holes" belonging to the basin of another attractor (or infinity).

In a real situation, a small noise that destroys the invariant synchronization subspace is unavoidable. Hence, the effect of the noise must be taken into consideration for any study of the loss of chaos synchronization. In the region of weak synchronization, due to local transverse repulsion of the repellers embedded in the SCA, a typical trajectory may have segments exhibiting positive local (finite-time) transverse Lyapunov exponents. For this case, any small noise results in a permanent intermittent bursting and a chaotic transient with a finite lifetime for the bursting and the riddling cases, respectively. The attractor bubbling and the chaotic transient demonstrate the sensitivity of the weakly stable SCA with respect to variations in the noise intensity. Recently, to characterize such noise sensitivity, we introduced a quantifier, called the noise sensitivity exponent (NSE), to measures the "degree" of noise sensitivity in coupled one-dimensional (1D) noninvertible maps [12]. The NSE is a quantitative characteristic of a weakly stable SCA, as in the case of the phase sensitivity exponent characterizing the degree of strangeness of strange nonchaotic attractors in quasiperiodic forced systems [13]. Here, we extend the method of characterizing the noise sensitivity in terms of the NSE to coupled high-dimensional invertible systems. As the coupling parameter is changed away from the point of the first transverse bifurcation, successive transverse bifurcations of periodic saddles embedded in the SCA occur. Hence, the value of the NSE increases because local transverse repulsions of the embedded periodic repellers strengthen.

This paper is organized as follows: In Sec. II, we char-

*E-mail: wclim@kwnu.kangwon.ac.kr

acterize the noise effect on weak synchronization in coupled Hénon maps and coupled pendula, which are representative models of coupled invertible systems. To measure the degree of noise sensitivity, we introduce the NSE and quantitatively characterize the noise sensitivity of a weakly stable SCA. In terms of the NSE, the noise effect on intermittent bursting and basin riddling is also characterized. Such a noise effect is found to be essentially the same as the effect of parameter mismatch between subsystems. Finally, a summary is given in Sec. III.

II. NOISE EFFECT IN COUPLED INVERTIBLE SYSTEMS

In this section, by extending the method proposed in coupled 1D noninvertible maps, we introduce the NSE in coupled Hénon maps and coupled pendula. We also quantitatively characterize the noise sensitivity of a weakly stable SCA. In terms of the NSEs, we characterize the effect of noise on the bubbling and the riddling.

1. Characterization of the Noise Effect in Coupled Hénon Maps

We first consider two coupled invertible Hénon maps, often used as a representative model for the Poincaré maps of coupled chaotic oscillators [14]:

$$T : \begin{cases} \mathbf{x}_{n+1} = \mathbf{F}(\mathbf{x}_n, \mathbf{y}_n) = \mathbf{f}(\mathbf{x}_n, a) + (1-\alpha)\, c\, \mathbf{g}(\mathbf{x}_n, \mathbf{y}_n) + \sigma \boldsymbol{\xi}_n, \\ \mathbf{y}_{n+1} = \mathbf{G}(\mathbf{x}_n, \mathbf{y}_n) = \mathbf{f}(\mathbf{y}_n, a) + c\, \mathbf{g}(\mathbf{y}_n, \mathbf{x}_n) + \sigma \boldsymbol{\eta}_n, \end{cases} \quad (1)$$

where $\mathbf{x}_n$ [$= (x_n^{(1)}, x_n^{(2)})$] and $\mathbf{y}_n$ [$= (y_n^{(1)}, y_n^{(2)})$] are state variables of the two subsystems at a discrete time n, the uncoupled dynamics ($c = 0$) is governed by the Hénon map with a nonlinearity parameter a and a damping parameter β ($|\beta| < 1$),

$$\mathbf{f}(\mathbf{x}, a) = (f(x^{(1)}, a) - x^{(2)}, \beta\, x^{(1)});\ \ f(x, a) = 1 - a\, x^2, \quad (2)$$

c is a coupling parameter between the two subsystems, and $\mathbf{g}(\mathbf{x}, \mathbf{y})$ is a coupling function of the form

$$\mathbf{g}(\mathbf{x}, \mathbf{y}) = (g(x^{(1)}, y^{(1)}), 0);\ \ g(x, y) = y^2 - x^2. \quad (3)$$

For $\alpha = 0$, the coupling is symmetric while for nonzero α ($0 < \alpha \leq 1$), it becomes asymmetric. The extreme case of asymmetric coupling with $\alpha = 1$ corresponds to unidirectional coupling. In such a way, α tunes the degree of asymmetry in the coupling. This asymmetric coupling naturally arises in the dynamics of two clusters for the case of global coupling, in which each element is coupled to all the other elements with equal strength [14]. For the ideal case without noise (*i.e.*, $\sigma = 0$), there exists an invariant synchronization plane, $x^{(1)} = y^{(1)}$ and $x^{(2)} = y^{(2)}$, in the $x^{(1)} - x^{(2)} - y^{(1)} - y^{(2)}$ phase space. However, in a real situation, noise is unavoidable; hence, the synchronization plane is no longer invariant. To take into consideration such a noise effect, one adds random variables $\boldsymbol{\xi}_n$ [$= (\xi_n^{(1)}, 0)$] and $\boldsymbol{\eta}_n$ [$= (\eta_n^{(1)}, 0)$] to Eq. (1). For this case, $\xi_n^{(1)}$ and $\eta_n^{(1)}$ are statistically independent random numbers chosen at each discrete time n from a uniform distribution with a zero mean $\langle \xi_n^{(1)} \rangle = \langle \eta_n^{(1)} \rangle = 0$ and a unit variance $\langle {\xi_n^{(1)}}^2 \rangle = \langle {\eta_n^{(1)}}^2 \rangle = 1$. Hence, $\xi_n^{(1)}$ and $\eta_n^{(1)}$ are just bounded random values uniformly distributed in the interval $[-\sqrt{3}, \sqrt{3}]$, and σ controls the "strength" of such a random noise.

As an example, we choose the unidirectionally coupled case of $\alpha = 1$ and fix the value of β at $\beta = 0.1$. For this case, the first master Hénon map with the state variable $\mathbf{x}$ can be regarded as a driver for the second slave Hénon map with the state variable $\mathbf{y}$ through the coupling term. For $a = 1.8$, we investigate the noise effect by changing the coupling parameter c. For this case, an SCA exists in the interval of $c_{b,l}[= -2.9974] < c < c_{b,r}[= -0.6026]$. As the coupling parameter c passes $c_{b,l}$ or $c_{b,r}$, the SCA becomes transversely unstable through a blowout bifurcation [14]; then, a complete desynchronization occurs. In the region of synchronization, a strongly stable SCA exists for $c_{t,l}[= -2.9] < c < c_{t,r}[= -0.7]$. For this case of strong synchronization, the SCA has no noise sensitivity because all periodic saddles embedded in the SCA are transversely stable. However, as the coupling parameter c passes $c_{t,r}$ and $c_{t,l}$, bubbling and riddling transitions, respectively, take place through the first transverse bifurcations of periodic saddles [7,8]; then, we have weak synchronization. For this case, the weakly stable SCA exhibits a noise sensitivity due to local transverse repulsion of the periodic repellers embedded in the SCA.

Hence, however small the noise intensity σ, a persistent intermittent bursting, called attractor bubbling, takes place in the region of bubbling ($c_{t,r} < c < c_{b,r}$). Such attractor bubbling is shown in Figs. 1(a) and 1(b) for $c = -0.62$ and $\sigma = 0.0001$. On the other hand, in the region of riddling ($c_{b,l} < c < c_{t,l}$), a weakly stable SCA with a riddled basin for $\sigma = 0$ is transformed into a chaotic transient (denoted by black dots) with a finite lifetime in the presence of noise, as shown in

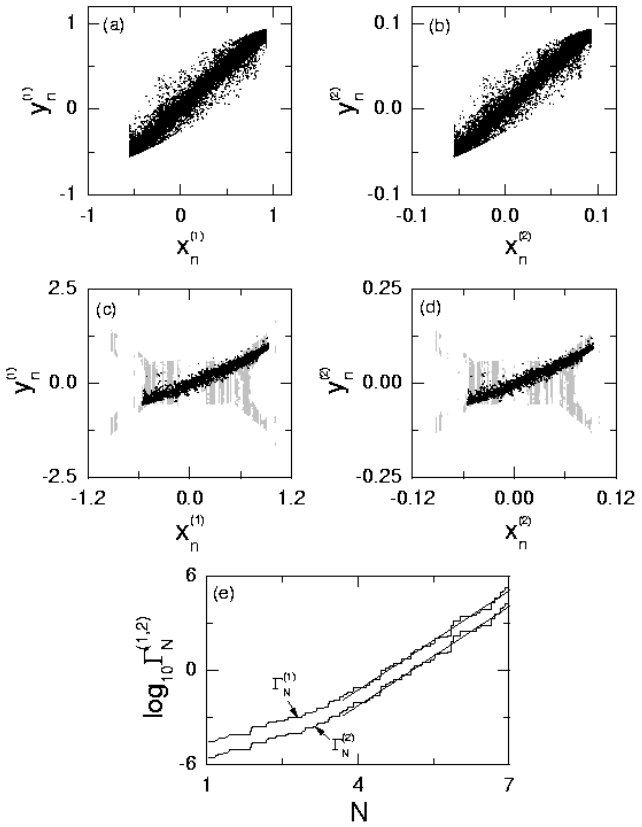

Fig. 1. Effect of noise with $\sigma = 0.0001$ on weak synchronization for $a = 1.8$ in unidirectionally coupled Hénon maps. For $c = -0.62$, projections of a bubbling attractor onto the (a) $x^{(1)} - y^{(1)}$ and (b) $x^{(2)} - y^{(2)}$ planes are given. In both (a) and (b), the initial orbit point is $(x^{(1)}, x^{(2)}, y^{(1)}, y^{(2)}) = (0.2, 0.02, 0.2, 0.02)$, the 5×10^3 points are computed before plotting, and the next 5×10^4 points are plotted. For the riddling case of $c = -2.99$, the SCA with a basin (gray region) riddled with a dense set of "holes" leading to divergent trajectories (white region) for $\sigma = 0$ is transformed into a chaotic transient (black dots). In (c) [(d)], a 2D slice with $x^{(2)} = y^{(2)} = 0.05$ [$x^{(1)} = y^{(1)} = 0.5$] through the 4D riddled basin of the weakly stable SCA is shown. Projections of a chaotic transient starting from an initial orbit point $(x^{(1)}, x^{(2)}, y^{(1)}, y^{(2)}) = (0.2, 0.02, 0.2, 0.02)$ onto the (c) $x^{(1)} - y^{(1)}$ and (d) $x^{(2)} - y^{(2)}$ planes are given. (e) Noise sensitivity functions $\Gamma_N^{(1)}$ and $\Gamma_N^{(2)}$ for $c = -0.62$, exhibiting asymptotic power-law behaviors are given. They are well fitted with straight lines with the same slope $\delta \simeq 2.15$.

Figs. 1(c) and 1(d) for $c = -2.99$. As c is varied away from $c_{t,l}$ or $c_{t,r}$, transversely unstable periodic repellers appear successively in the SCA via transverse bifurcations. Then, the degree of the noise sensitivity of the SCA increases because local transverse repulsion of the periodic repellers embedded in the SCA becomes strong.

To quantitatively characterize the noise sensitivity of the weakly stable SCA, we consider an orbit $\{(\mathbf{x}_n, \mathbf{y}_n)\}$ starting from an initial point on the synchronization plane (*i.e.*, $\mathbf{x}_0 = \mathbf{y}_0$). As the strength of the local transverse repulsion from the synchronization plane increases, the SCA becomes more and more sensitive with respect to the variation of σ. Such noise sensitivity of the SCA for $\sigma = 0$ may be characterized by calculating the derivative of the transverse variable $\mathbf{u}_n$ $(= \mathbf{x}_n - \mathbf{y}_n)$, denoting the deviation from the synchronization plane, with respect to σ (*i.e.*, $\left.\frac{\partial \mathbf{u}_{n+1}}{\partial \sigma}\right|_{\sigma=0} = \left.\frac{\partial \mathbf{x}_{n+1}}{\partial \sigma}\right|_{\sigma=0} - \left.\frac{\partial \mathbf{y}_{n+1}}{\partial \sigma}\right|_{\sigma=0}$). Using Eq. (1), we obtain the following recurrence relation:

$$\left.\frac{\partial \mathbf{u}_{n+1}}{\partial \sigma}\right|_{\sigma=0} = r(\mathbf{x}_n^*) \left.\frac{\partial \mathbf{u}_n}{\partial \sigma}\right|_{\sigma=0} + \boldsymbol{\zeta}_n, \tag{4}$$

where $\left.\frac{\partial \mathbf{u}_n}{\partial \sigma}\right|_{\sigma=0} = \left(\left.\frac{\partial u_n^{(1)}}{\partial \sigma}\right|_{\sigma=0}, \left.\frac{\partial u_n^{(2)}}{\partial \sigma}\right|_{\sigma=0} \right)$, the 2×2 matrix $r(\mathbf{x}_n^*)$ is given by

$$r(\mathbf{x}_n^*) \equiv \begin{pmatrix} f_{x^{(1)}}(x_n^{(1)*}, a) - (2-\alpha) c\, h(x_n^{(1)*}) & -1 \\ \beta & 0 \end{pmatrix} \tag{5}$$

and

$$\boldsymbol{\zeta}_n \equiv \boldsymbol{\xi}_n - \boldsymbol{\eta}_n = \begin{pmatrix} \xi_n^{(1)} - \eta_n^{(1)} \\ 0 \end{pmatrix}. \tag{6}$$

Here, f_x is the derivatives of $f(x, a)$ with respect to x, $\{(\mathbf{x}_n^*, \mathbf{y}_n^*)\}$ is a synchronous orbit with $\mathbf{x}_n^* = \mathbf{y}_n^*$ for $\sigma = 0$, $h(x)$ is a reduced coupling function defined by [15]

$$h(x) \equiv \left.\frac{\partial g(x, y)}{\partial y}\right|_{y=x}, \tag{7}$$

and $\zeta_n^{(1)} (\equiv \xi_n^{(1)} - \eta_n^{(1)})$ are random numbers chosen from the bounded distribution density function, $P(\zeta^{(1)}) = -\frac{1}{12}|\zeta^{(1)}| + \frac{\sqrt{3}}{6}$ in the interval $[-2\sqrt{3}, 2\sqrt{3}]$. Hence, starting from an initial orbit point $(\mathbf{x}_0^*, \mathbf{y}_0^*)$ on the synchronization plane, we may obtain derivatives at all points of the orbit:

$$\left.\frac{\partial \mathbf{u}_N}{\partial \sigma}\right|_{\sigma=0} = \sum_{k=1}^{N} R_{N-k}(\mathbf{x}_k^*) \boldsymbol{\zeta}_{k-1} + R_N(\mathbf{x}_0^*) \left.\frac{\partial \mathbf{u}_0}{\partial \sigma}\right|_{\sigma=0}, \tag{8}$$

where

$$R_M(\mathbf{x}_m^*) = \prod_{i=0}^{M-1} r(\mathbf{x}_{m+i}^*), \tag{9}$$

which is a product of the "transverse Jacobian matrices" $r(\mathbf{x}^*)$ determining the stability against a perturbation transverse to the synchronization plane and $R_0 = I$ (identity matrix). Note that the eigenvalues, $\lambda_M^{T,1}(\mathbf{x}_m^*)$ and $\lambda_M^{T,2}(\mathbf{x}_m^*)$ ($|\lambda_M^{T,1}(\mathbf{x}_m^*)| \geq |\lambda_M^{T,2}(\mathbf{x}_m^*)|$) of $R_M(\mathbf{x}_m^*)$ are associated with the local (M-time) transverse Lyapunov exponents $\sigma_M^{T,1}$ and $\sigma_M^{T,2}$ ($\sigma_M^{T,1} \geq \sigma_M^{T,2}$) of the SCA that are averaged over M synchronous orbit points starting from $\mathbf{x}_m^*$ as follows:

$$\sigma_M^{T,i}(\mathbf{x}_m^*) = \frac{1}{M} \ln |\lambda_M^{T,i}(\mathbf{x}_m^*)|, (i = 1, 2). \tag{10}$$

Thus, $\lambda_M^{T,1}$ and $\lambda_M^{T,2}$ become local (transverse stability) multipliers that determine the local sensitivity of the motion during a finite time M. As $M \to \infty$, $\sigma_M^{T,1}$ approaches the largest transverse Lyapunov exponent $\sigma_T^{(1)}$, which denotes the average exponential rate of divergence of an infinitesimal perturbation transverse to the SCA. Equation (8) reduces to

$$\left.\frac{\partial \mathbf{u}_N}{\partial \sigma}\right|_{\sigma=0} = \mathbf{S}_N^{(n)}(\mathbf{x}_0^*) \equiv \sum_{k=1}^{N} R_{N-k}(\mathbf{x}_k^*)\boldsymbol{\zeta}_{k-1}, \qquad (11)$$

because $\left.\frac{\partial \mathbf{u}_0}{\partial \sigma}\right|_{\sigma=0} = 0$. Since the values of $\boldsymbol{\zeta}$ are bounded, the boundedness of the partial sum $\mathbf{S}_N^{(n)}$ is determined just by the largest eigenvalues $\lambda_M^{T,1}$ of R_M.

For the case of weak synchronization, transversely unstable periodic repellers are embedded in the SCA. When a typical trajectory visits neighborhoods of such repellers, it has segments experiencing local repulsion from the synchronization plane. Thus, the distribution of the largest local transverse Lyapunov exponents $\sigma_M^{T,1}$ for a large ensemble of trajectories and for large M may have a positive tail [16]. For the segments of a trajectory exhibiting a positive largest local transverse Lyapunov exponent ($\sigma_M^{T,1} > 0$), the largest local transverse multipliers $\lambda_M^{T,1}$ [$= \pm\exp(\sigma_M^{T,1} M)$] can be arbitrarily large; hence, the partial sums $S_N^{n,i}$ ($i = 1, 2$) may be arbitrarily large. This implies unbounded growth of the derivatives $\left.\frac{\partial u_N^{(i)}}{\partial \sigma}\right|_{\sigma=0}$ ($i = 1, 2$) as N tends to infinity; consequently, the weakly stable SCA has a noise sensitivity.

As an example, we consider the weakly stable SCA for $c = -0.62$. If we iterate Eq. (4) with $\left.\frac{\partial \mathbf{u}_0}{\partial \sigma}\right|_{\sigma=0} = \mathbf{0}$ along a synchronous trajectory starting from an initial orbit point $(\mathbf{x}_0^*, \mathbf{y}_0^*)$ on the synchronization plane, then we obtain the partial sum $\mathbf{S}_N^{(n)}(\mathbf{x}_0^*)$ of Eq. (11). The partial sum $S_N^{n,i}$ $\left[= \left.\frac{\partial u_N^{(i)}}{\partial \sigma}\right|_{\sigma=0}\right]$ ($i = 1, 2$) becomes very intermittent. However, by looking only at the maximum

$$\gamma_N^{(i)}(x_0^*) = \max_{0 \le k \le N} |S_k^{n,i}(\mathbf{x}_0^*)| \ \ (i = 1, 2), \qquad (12)$$

one can easily see the boundedness of $S_N^{n,i}$. For this case, $\gamma_N^{(1)}$ and $\gamma_N^{(2)}$ grow unboundedly. Consequently, the weakly stable SCA has a noise sensitivity. The growth rate of the function $\gamma_N^{(i)}(\mathbf{x}_0^*)$ with time N represents the degree of noise sensitivity and can be used as a quantitative characteristic of the weakly stable SCA. However, $\gamma_N^{(i)}(\mathbf{x}_0^*)$ depends on a particular trajectory. To obtain a representative quantity, we consider an ensemble of randomly chosen initial points $(\mathbf{x}_0^*, \mathbf{y}_0^*)$ on the synchronization plane and take the minimum value of $\gamma_N^{(i)}$ with respect to the initial orbit points,

$$\Gamma_N^{(i)} = \min_{\mathbf{x}_0^*} \gamma_N^{(i)}(\mathbf{x}_0^*) \ \ (i = 1, 2). \qquad (13)$$

Figure 1(e) shows the noise sensitivity functions $\Gamma_N^{(1)}$ and $\Gamma_N^{(2)}$. Note that $\Gamma_N^{(1)}$ and $\Gamma_N^{(2)}$ grow unboundedly with the same power δ,

$$\Gamma_N^{(i)} \sim N^{\delta} \text{ for } i = 1, 2, \qquad (14)$$

because their growth is governed by the same largest local multipliers $\lambda_M^{T,1}$. Here, the value of $\delta \simeq 2.15$ is a quantitative characteristic of the noise sensitivity of the SCA for $c = -0.62$, and we call it the NSE.

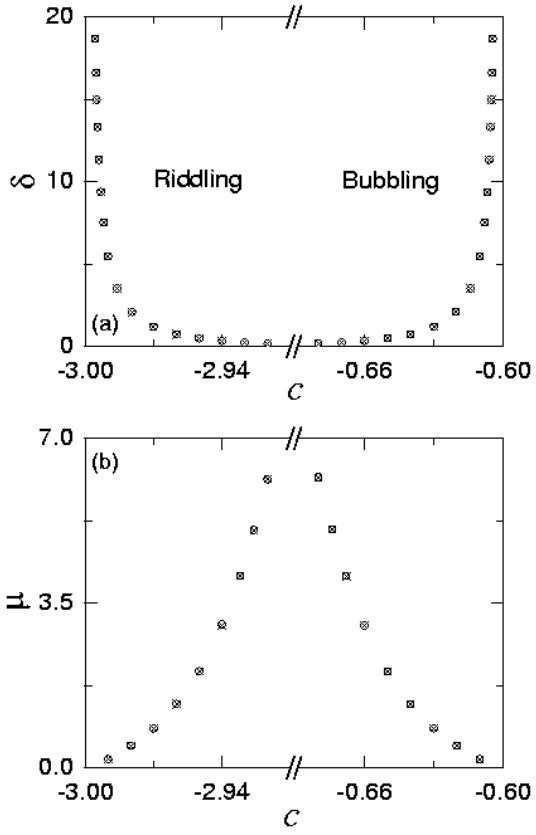

Fig. 2. (a) Plot of the NSEs δ (circles) versus c for $a = 1.8$ in unidirectionally coupled Hénon maps. Note that the values of the NSE are the same as those of the parameter sensitivity exponents (crosses) within the numerical accuracy. (b) Plot of the scaling exponents μ (circles) for the average characteristic time versus c for $a = 1.8$. They agree well the reciprocals of the NSEs (crosses).

In each region of bubbling or riddling, we obtain the NSEs by varying the coupling parameter c from the bubbling or the riddling transition point to the blowout bifurcation point. For obtaining a satisfactory statistics, we consider 100 ensembles for each c, each of which contains 100 randomly chosen initial orbit points on the synchronization plane, and we choose the average value of the 100 NSEs obtained in the 100 ensembles. Figure 2(a) shows the plot of such NSEs (denoted by circles) versus c. As explained above, the NSEs are determined by the largest local transverse Lyapunov exponents, $\sigma_M^{T,1}$, of the SCA. In the coupled Hénon maps, $\sigma_M^{T,1}$ is symmetric with respect to a center $c = c^*$ [$= -a(= -1.8)$], at which the value of $\sigma_M^{T,1}$ is minimum. As c increases or

decreases from c^*, the value of $\sigma_M^{T,1}$ increases symmetrically. Hence, the NSE in Fig. 2(a) becomes symmetric about $c = c^*$, and it tends to infinity as c approaches the blowout bifurcation point. This increase in the noise sensitivity of the SCA is caused by an increase in the strength of the local transverse repulsion of periodic repellers embedded in the SCA. After the blowout bifurcation, the weakly stable SCA becomes transversely unstable; hence, a complete desynchronization occurs.

We now compare the formula in Eq. (11) for the partial sum $\mathbf{S}_N^{(n)}$ with the following analogous formula for $\mathbf{S}_N^{(p)}$ that was obtained in the parameter-mismatching case [17]:

$$\left.\frac{\partial \mathbf{u}_N}{\partial \varepsilon}\right|_{\varepsilon=0} = \mathbf{S}_N^{(p)}(\mathbf{x}_0^*) \equiv \sum_{k=1}^{N} R_{N-k}(\mathbf{x}_k^*)\mathbf{f}_a(\mathbf{x}_{k-1}^*, a), \quad (15)$$

where ε is a mismatching parameter and $\mathbf{f}_a(\mathbf{x}_{k-1}^*, a) = (f_a(x_{k-1}^{(1)*}, a), 0)$. Here, f_a is the derivative of $f(x, a)$ with respect to a, and R_M is given in Eq. (9). As in the case of noise, the weakly stable SCA exhibits a parameter sensitivity because of the unbounded growth of the partial sum $\mathbf{S}_N^{(p)}$ with N. Since the derivative values $f_a(x_{k-1}^{(1)*}, a)$ $[= -(x_{k-1}^{(1)*})^2\ ]$ are bounded in the interval $[-1, 0]$, the boundedness of the partial sum $\mathbf{S}_N^{(p)}$ is also determined by the (same) largest eigenvalues $\lambda_M^{T,1}$ of R_M, as in the case of noise. This implies that the noise sensitivity function grows unboundedly with the same power as in the parameter-mismatching case. Hence, the values of the NSE (denoted by circles) become the same as those of the parameter sensitivity exponent (denoted by crosses), as shown in Fig. 2(a). We note that this is a general result and is valid for any bounded noise.

In terms of the NSEs, we also characterize the noise effect on the bubbling and the riddling of a weakly stable SCA. In the presence of noise, the weakly stable SCA is transformed into a bubbling attractor or a chaotic transient, depending on the global dynamics. For this case, the quantity of interest is the average time τ spent near the synchronization plane. For the case of the bubbling attractor, τ is the average interburst time, while for the case of the chaotic transient, τ is its average lifetime. As c is changed from the bubbling or the riddling transition point, τ becomes short because the local transverse repulsion of periodic repellers embedded in the SCA becomes stronger.

For the case of bubbling, the bubbling attractor is in the laminar phase when the magnitude of the deviation from the synchronization plane, d_n $[\equiv (|u_n^{(1)}| + |u_n^{(2)}|)/2]$, is less than a threshold value d_b^* (*i.e.*, $d_n < d_b^*$). Otherwise, it is in the bursting phase. Here, d_b^* is very small compared to the maximum bursting amplitude, and it is the maximum deviation from the synchronization plane that may be acceptable in the context of synchronization. For each c, we follow the trajectory starting from the initial orbit point $(0.2, 0.02, 0.2, 0.02)$ until 50,000 laminar phases are obtained; then, we get the average laminar length τ (*i.e.*, the average interburst interval) that scales with σ as [18]

$$\tau \sim \sigma^{-\mu}. \quad (16)$$

The plot of the scaling exponent μ (denoted by circles) versus c is shown in Fig. 2(b). As c increases, the value of μ decreases because the average laminar length shortens.

For each c in the region of riddling, we consider an ensemble of trajectories starting from 1000 randomly chosen initial points on the synchronization plane and obtain the average lifetime of the chaotic transients. A trajectory may be regarded as having escaped once the magnitude of deviation d_n from the synchronization plane becomes larger than a threshold value d_c^* such that an orbit point with $d > d_c^*$ lies sufficiently outside the basin of the SCA. Thus, the average lifetime τ is found to scale with σ as [18]

$$\tau \sim \sigma^{-\mu}. \quad (17)$$

The plot of the scaling exponent μ (denoted by circles) versus c is given in Fig. 2(b). As c decreases toward the blowout bifurcation point, the average lifetime shortens; hence, the value of μ decreases.

We note that the scaling exponent μ is associated with the NSE δ as follows: For a given σ, consider a trajectory starting from a randomly chosen initial orbit point on the synchronization plane. Then, from Eq. (14), the "average" time τ at which the magnitude of the deviation from the synchronization plane becomes the threshold value $d_{b,c}^*$ can be obtained as

$$\tau \sim \sigma^{-1/\delta}. \quad (18)$$

Hence, the scaling exponent μ for τ is given by the reciprocal of the NSE δ,

$$\mu = 1/\delta. \quad (19)$$

The reciprocal values of δ (denoted by crosses) are also plotted in Fig. 2(b), and they agree well with the values of μ (denoted by circles). The same reciprocal relation between the scaling exponent for the average characteristic time τ and the parameter sensitivity exponent exists in the parameter-mismatching case [17]. Thus, the values of the scaling exponents in both the cases of noise and parameter mismatch become the same because the values of the NSE and the parameter sensitivity exponent are the same. Consequently, noise and parameter mismatch have the same effect on the scaling behavior of the average characteristic time τ.

2. Characterization of the Noise Effect in Coupled Pendula

As a second example, we consider an invertible system of two coupled parametrically forced pendula [14]:

$$\begin{aligned} \dot{\mathbf{x}} &= \mathbf{F}(\mathbf{x}, \mathbf{y}) = \mathbf{f}(\mathbf{x}, a) + (1-\alpha)\, c\, \mathbf{g}(\mathbf{x}, \mathbf{y}) + \sigma \boldsymbol{\xi}, \\ \dot{\mathbf{y}} &= \mathbf{G}(\mathbf{x}, \mathbf{y}) = \mathbf{f}(\mathbf{y}, a) + c\, \mathbf{g}(\mathbf{y}, \mathbf{x}) + \sigma \boldsymbol{\eta}, \end{aligned} \quad (20)$$

where the overdot denotes differentiation with respect to time, $\mathbf{x}$ [$= (x^{(1)}, x^{(2)})$] and $\mathbf{y}$ [$= (y^{(1)}, y^{(2)})$] are state variables of the two subsystems, c is a coupling parameter between the subsystems, α ($0 \leq \alpha \leq 1$) is a parameter tuning the degree of asymmetry of the coupling, and $\mathbf{g}(\mathbf{x}, \mathbf{y})$ is a coupling function of the form

$$\mathbf{g}(\mathbf{x}, \mathbf{y}) = (g(x^{(1)}, y^{(1)}), g(x^{(2)}, y^{(2)})); \\ g(x, y) = y - x. \quad (21)$$

Here, the uncoupled dynamics ($c = 0$) is governed by a parametrically forced pendulum:

$$\mathbf{f}(\mathbf{x}, a) = (x^{(2)}, f(x^{(1)}, x^{(2)}, a)); \\ f(x^{(1)}, x^{(2)}, a) \\ = -2\pi\beta\Omega\, x^{(2)} - 2\pi(\Omega^2 - a\cos 2\pi t)\sin 2\pi x^{(1)}, \quad (22)$$

where $x^{(1)}$ is a normalized angle with range $x^{(1)} \in [0, 1)$, $x^{(2)}$ is a normalized angular velocity, β is a normalized damping parameter, Ω is a normalized natural frequency of the unforced pendulum, and a is a normalized driving amplitude of the vertical oscillation of the suspension point. As in the case of the two coupled Hénon maps, these two coupled pendula may also be used as a model for investigating two-cluster dynamics in many globally coupled pendula.

The phase space of the coupled parametrically forced pendula is five dimensional with coordinates $x^{(1)}$, $x^{(2)}$, $y^{(1)}$, $y^{(2)}$, and t. Since the system is periodic in t, it is convenient to regard time as a circular coordinate in phase space. We also consider the surface of the section, the $x^{(1)}$- $x^{(2)}$-$y^{(1)}$-$y^{(2)}$ hypersurface, at integer times (*i.e.*, $t = m$, m: integer). Then, using the Heun method (corresponding to the 2nd-order Runge-Kutta method) [19] with a time step $h = 0.05$, we integrate the stochastic differential equations of Eq. (20) and follow a trajectory. This phase-space trajectory intersects the surface of the section in a sequence of points. This sequence of points corresponds to a mapping on the 4D hypersurface. The map can be computed by stroboscopically sampling the orbit points $\mathbf{z}_m$ [$\equiv (x^{(1)}(m), x^{(2)}(m), y^{(1)}(m), y^{(2)}(m))$] at the discrete time m. We call the transformation $\mathbf{z}_m \to \mathbf{z}_{m+1}$ the Poincaré map and write $\mathbf{z}_{m+1} = P(\mathbf{z}_m)$.

As an example, we consider the 4D Poincaré map P for the unidirectionally coupled case of $\alpha = 1$ and fix the values of β and Ω at $\beta = 1.0$ and $\Omega = 0.5$. For the ideal case without noise (*i.e.*, $\sigma = 0$), there exists an invariant synchronization plane, $x^{(1)} = y^{(1)}$ and $x^{(2)} = y^{(2)}$, in the $x^{(1)}$-$x^{(2)}$-$y^{(1)}$-$y^{(2)}$ phase space. However, in a real situation, noise is unavoidable; hence, the synchronization plane is no longer invariant. To take into consideration such noise effect, one adds random variables $\boldsymbol{\xi}$ [$= (\xi^{(1)}, \xi^{(2)})$] and $\boldsymbol{\eta}$ [$= (\eta^{(1)}, \eta^{(2)})$] to Eq. (20). For this case, $\xi^{(i)}$ and $\eta^{(i)}$ ($i = 1, 2$) are Gaussian white noises with a zero mean $\langle\xi^{(i)}(t)\rangle = \langle\eta^{(i)}(t)\rangle = 0$ and a delta correlation $\langle\xi^{(i)}(t_1)\,\xi^{(j)}(t_2)\rangle = \delta_{ij}\,\delta(t_1 - t_2)$, $\langle\eta^{(i)}(t_1)\,\eta^{(j)}(t_2)\rangle = \delta_{ij}\,\delta(t_1 - t_2)$, and $\langle\xi^{(i)}(t_1)\,\eta^{(j)}(t_2)\rangle = 0$, and σ controls the "strength" of such a random noise.

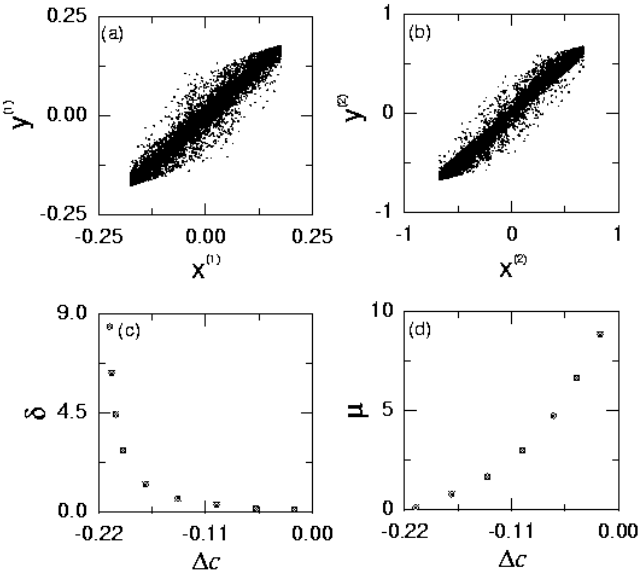

Fig. 3. Effect of noise on weak synchronization for $a = 0.85$ in the 4D Poincaré map of unidirectionally coupled pendula. For $c = 0.67$ and $\sigma = 0.0001$, projections of a bubbling attractor onto the (a) $x^{(1)} - y^{(1)}$ and (b) $x^{(2)} - y^{(2)}$ planes are given. In both (a) and (b), the initial orbit point is $(x^{(1)}, x^{(2)}, y^{(1)}, y^{(2)}) = (0.1, 0.3, 0.1, 0.3)$, the 5×10^3 points are computed before plotting, and the next 5×10^4 points are plotted. (c) Plot of the NSEs δ (circles) versus Δc ($= c - c_t$). The values of the NSE are the same as those of the parameter sensitivity exponent (crosses) within the numerical accuracy. (d) Plot of the scaling exponents μ (circles) for the average interburst interval versus Δc. They agree well the reciprocals of the NSEs (crosses).

For $a = 0.85$, we investigate the noise effect by varying the coupling parameter c. For this case, a SCA exists for $c > c_b$[$\simeq 0.648$]. As the coupling parameter c passes c_b, the SCA becomes transversely unstable via a blowout bifurcation; then, a complete desynchronization occurs. In the region of synchronization, a strongly stable SCA without noise sensitivity exists for $c > c_t$[$= 0.858\,688$] because all periodic saddles embedded in the SCA are transversely stable. However, as the coupling parameter c passes c_t, a bubbling transition occurs through the first transverse bifurcation of a periodic saddle; then, we have weak synchronization. For this case, the weakly stable SCA has a noise sensitivity due to the local transverse repulsion of the periodic repellers embedded in the SCA. Hence, only attractor bubbling occurs in the region of weak synchronization ($c_b < c < c_t$), as shown in Figs. 3(a) and 3(b) for $c = 0.67$ and $\sigma = 0.0001$.

We extend the method proposed in coupled 1D maps to coupled pendula and quantitatively characterize the noise sensitivity of a weakly stable SCA. Such noise sensitivity of the SCA for $\sigma = 0$ may be characterized by calculating the derivative of the transverse variable $\mathbf{u}$ ($= \mathbf{x} - \mathbf{y}$), denoting the deviation from the synchronization plane, with respect to σ (*i.e.*, $\frac{\partial \mathbf{u}}{\partial \sigma}\big|_{\sigma=0} =$

$\frac{\partial \mathbf{x}}{\partial \sigma}\big|_{\sigma=0} - \frac{\partial \mathbf{y}}{\partial \sigma}\Big|_{\sigma=0}$). Using Eq. (20), we obtain the following governing equation for $\frac{\partial \mathbf{u}}{\partial \sigma}\big|_{\sigma=0}$:

$$\left.\frac{\partial \dot{\mathbf{u}}}{\partial \sigma}\right|_{\sigma=0} = r(\mathbf{x}^*)\left.\frac{\partial \mathbf{u}}{\partial \sigma}\right|_{\sigma=0} + \boldsymbol{\zeta}, \tag{23}$$

$$r(\mathbf{x}^*) \equiv \begin{pmatrix} -(2-\alpha)\,c\,h(x^{(1)*}) & 1 \\ f_{x^{(1)}}(x^{(1)}, x^{(2)}, a) & f_{x^{(2)}}(x^{(1)}, x^{(2)}, a) - (2-\alpha)\,c\,h(x^{(2)*}) \end{pmatrix}, \tag{24}$$

and $\boldsymbol{\zeta} \equiv \boldsymbol{\xi} - \boldsymbol{\eta}$. Here, $f_{x^{(1)}}$ and $f_{x^{(2)}}$ are the derivatives of $f(x^{(1)}, x^{(2)}, a)$ with respect to $x^{(1)}$ and $x^{(2)}$, $\{(\mathbf{x}_n^*, \mathbf{y}_n^*)\}$ is a synchronous orbit with $\mathbf{x}_n^* = \mathbf{y}_n^*$ for $\sigma = 0$, and $h(x)$ $\left[\equiv \frac{\partial g(x,y)}{\partial y}\Big|_{y=x}\right]$ is a reduced coupling function. Integrating the formula in Eq. (23) along a synchronous trajectory starting from an initial orbit point $(\mathbf{x}_0^*, \mathbf{y}_0^*)$ on the synchronization plane and an initial value $\frac{\partial \mathbf{u}}{\partial \sigma}\big|_{\sigma=0} = \mathbf{0}$ for $t = 0$, we may obtain derivatives $\mathbf{S}_n^{(n)}(\mathbf{x}^*)$ $(\equiv \frac{\partial \mathbf{u}}{\partial \sigma}\big|_{\sigma=0})$ at all subsequent discrete times $t = n$. Then, following the same procedure for the coupled Hénon maps, one can get the NSE δ of Eq. (14), which measures the degree of noise sensitivity of the SCA.

In the region of bubbling, we obtain the NSEs by changing the coupling parameter c from the bubbling transition point c_t to the blowout bifurcation point c_b. To obtain satisfactory statistics, we consider 100 ensembles for each c, each of which contains 20 randomly chosen initial orbit points on the synchronization plane, and we choose the average value of the 100 NSEs obtained in the 100 ensembles. Figure 3(c) shows a plot of such NSEs (denoted by circles) versus Δc $(\equiv c - c_t)$. Note that the NSE δ monotonically increases as c is changed away from the bubbling transition point and tends to infinity as c approaches the blowout bifurcation point. This increase in the noise sensitivity of the SCA is caused by an increase in the strength of the local transverse repulsion of periodic repellers embedded in the SCA. We also note that, for the coupled Hénon maps, the values of the NSE (denoted by circles) are the same as those of the parameter sensitivity exponent (denoted by crosses) [see Fig. 3(c)] because the random variable $\boldsymbol{\zeta}$ in Eq. (23) is bounded. In terms of the NSEs, we also characterize the noise effect on the bubbling of a weakly stable attractor. For each c, we follow the trajectory starting from an initial orbit point $(0.1, 0.3, 0.1, 0.3)$ until 50,000 laminar phases are obtained; then, we find that the average laminar length τ exhibits a power-law scaling behavior as in Eq. (16). A plot of the scaling exponent μ (circles) versus Δc $(\equiv c - c_t)$ is shown in Fig. 3(d). As c decreases from c_t, the value of μ decreases because the average laminar length shortens. As in the case of the coupled Hénon maps, the scaling exponent μ is given by the reciprocal of the NSE δ [see Eq. (19)]. The reciprocal values of δ (denoted by crosses) are also plotted in Fig. 3(d). Note that they agree well with the values of μ (denoted by circles). The same reciprocal relation between the scaling exponent μ and the parameter sensitivity exponent exists in the parameter-mismatching case. Since the values of the NSE and the parameter sensitivity exponent are the same, noise and parameter mismatch have the same effect on the scaling behavior of the average characteristic time τ.

So far, in both systems, coupled Hénon maps and coupled pendula, we have characterized the noise effect in the unidirectionally coupled case with an asymmetry parameter $\alpha = 1$. Through Eqs. (5) and (24), one can easily see that the NSE for a given (a, c) in the case of $\alpha = 1$ is the same as that for the value of $[a, c/(2-\alpha)]$ in other cases with $0 \le \alpha < 1$. Thus, the results for the NSEs given in Figs. 2(a) and 3(c) may be converted into those for the case of general α only by a scale change in the coupling parameter such that $c \to c/(2-\alpha)$.

III. SUMMARY

By extending the method proposed in coupled 1D noninvertible maps, we have investigated the effect of noise on weak synchronization in coupled Hénon maps and coupled pendula, which are high-dimensional invertible systems. Because of the existence of local positive transverse Lyapunov exponents, a weakly stable SCA exhibits a sensitivity with respect to variations in the noise intensity, as in the case of the parameter mismatch. To measure the degree of such noise sensitivity, we introduced a quantifier, called the NSE, and quantitatively characterized the noise sensitivity of a weakly stable SCA. For both noise and parameter mismatch, the degree of sensitivity is determined only by the (same) local transverse Lyapunov exponents of the "unperturbed" SCA in the absence of noise and parameter mismatch. Hence, both the NSE and the parameter sensitivity exponent become the same, independently of the detailed properties of the noise and the parameter mismatch, because the roles of the noise and the parameter mismatch are just to break the invariant synchronization plane. Thus,

the noise and the parameter mismatch have the same effect on the scaling behavior of the average characteristic time of the bubbling attractor and the chaotic transient.

ACKNOWLEDGMENTS

This work was supported by the Korea Science and Engineering Foundation (Grant No. R05-2003-000-10045-0).

REFERENCES

[1] K. M. Cuomo and A. V. Oppenheim, Phys. Rev. Lett. **71**, 65 (1993); L. Kocarev, K. S. Halle, K. Eckert, L. O. Chua and U. Parlitz, Int. J. Bifurcation Chaos Appl. Sci. Eng. **2**, 973 (1992); L. Kocarev and U. Parlitz, Phys. Rev. Lett. **74**, 5028 (1995); N. F. Rulkov, Chaos **6**, 262 (1996).

[2] H. Fujisaka and T. Yamada, Prog. Theor. Phys. **69**, 32 (1983); A. S. Pikovsky, Z. Phys. B: Condens. Matter **50**, 149 (1984); V. S. Afraimovich, N. N. Verichev and M. I. Rabinovich, Radiophys. Quantum Electron. **29**, 795 (1986); L. M. Pecora and T. L. Carroll, Phys. Rev. Lett. **64**, 821 (1990).

[3] P. Ashwin, J. Buescu and I. Stewart, Nonlinearity **9**, 703 (1996).

[4] B. R. Hunt and E. Ott, Phys. Rev. Lett. **76**, 2254 (1996); Phys. Rev. E **54**, 328 (1996).

[5] Y.-C. Lai, C. Grebogi, J. A. Yorke and S. C. Venkataramani, Phys. Rev. Lett. **77**, 55 (1996).

[6] V. Astakhov, A. Shabunin, T. Kapitaniak and V. Anishchenko, Phys. Rev. Lett. **77**, 55 (1996).

[7] Yu. L. Maistrenko, V. L. Maistrenko, O. Popovich and E. Mosekilde, Phys. Rev. E **57**, 2713 (1998); **60**, 2817 (1999); O. Popovych, Yu. L. Maistrenko, E. Mosekilde, A. Pikovsky and J. Kurths, Phys. Rev. E **63**, 036201 (2001).

[8] S.-Y. Kim and W. Lim, Phys. Rev. E **63**, 026217 (2001); *ibid.* **64**, 016211 (2001); J. Phys. A **36**, 6951 (2003); S.-Y. Kim, W. Lim and Y. Kim, Prog. Theor. Phys. **105**, 187 (2001).

[9] P. Ashwin, J. Buescu and I. Stewart, Phys. Lett. A **193**, 126 (1994); J. F. Heagy, T. L. Carroll and L. M. Pecora, Phys. Rev. E **52**, 1253 (1995); D. J. Gauthier and J. C. Bienfang, Phys. Rev. Lett. **77**, 1751 (1996); V. Ashtakhov, M. Hasler, T. Kapitaniak, V. Shabunin and V. Anishchenko, Phys. Rev. E **58**, 5620 (1998); S. Yanchuk, Y. Maistrenko, B. Lading and E. Mosekilde, Int. J. Bifurcation Chaos Appl. Sci. Eng. **10**, 2629 (2000); S.-Y. Kim and W. Lim, J. Phys. A **36**, 6951 (2003).

[10] C. Venkataramani, B. R. Hunt and E. Ott, Phys. Rev. E **54**, 1346 (1996); S. C. Venkataramani, B. R. Hunt, E. Ott, D. J. Gauthier and J. C. Bienfang, Phys. Rev. Lett. **77**, 5361 (1996); A. V. Zimin, B. R. Hunt and E. Ott, Phys. Rev. E **67**, 016204 (2003).

[11] J. C. Alexander, J. A. Yorke, Z. You and I. Kan, Int. J. Bifurcation Chaos Appl. Sci. Eng. **2**, 795 (1992); E. Ott, J. C. Sommerer, J. C. Alexander, I. Kan and J. A. Yorke, Phys. Rev. Lett. **71**, 4134 (1993); J. C. Sommerer and E. Ott, Nature (London) **365**, 136 (1993); E. Ott, J. C. Alexander, I. Kan, J. C. Sommerer and J. A. Yorke, Physica D **76**, 384 (1994); J. F. Heagy, T. L. Carroll and L. M. Pecora, Phys. Rev. Lett. **73**, 3528 (1994).

[12] S.-Y. Kim, W. Lim, A. Jalnine and S. P. Kuznetsov, Phys. Rev. E **67**, 016217 (2003).

[13] A. Pikovsky and U. Feudel, Chaos **5**, 253 (1995).

[14] S.-Y. Kim, W. Lim, E. Ott and B. Hunt, Phys. Rev. E **68**, 066203 (2003).

[15] S.-Y. Kim and H. Kook, Phys. Rev. A **48**, 785 (1993).

[16] A. Jalnine and S.-Y. Kim, Phys. Rev. E **65**, 026210 (2002).

[17] W. Lim and S.-Y. Kim, J. Korean Phys. Soc. **44**, 510 (2004)

[18] S.-Y. Kim, W. Lim and Y. Kim, Prog. Theor. Phys. **107**, 2 (2002).

[19] M. San Miguel and R. Toral, *Stochastic Effects in Physical Systems* in *Instabilities and Nonequilibrium Structures VI*, editted by E. Tirapegui and W. Zeller (Kluwer Press, 1999).